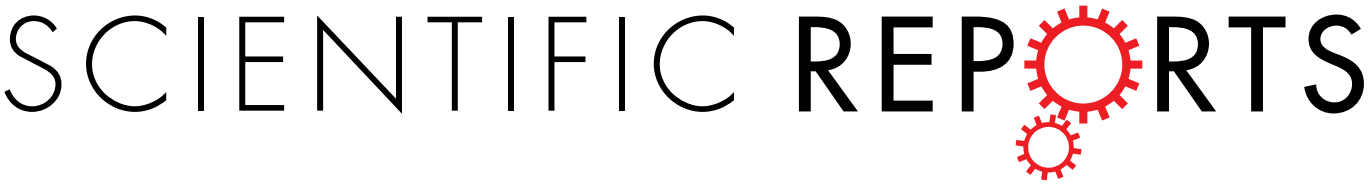

OPEN

Solvent and Intermediate Phase as Boosters for the Perovskite Transformation and Solar Cell Performance

Received: 14 December 2015
Accepted: 20 April 2016
Published: 09 May 2016

Jinhyun Kim[1], Taehyun Hwang[1], Sangheon Lee[1], Byungho Lee[1], Jaewon Kim[1], Gil Su Jang[1], Seunghoon Nam[2] & Byungwoo Park[1]

High power conversion efficiency and device stabilization are two major challenges for $CH_3NH_3PbI_3$ ($MAPbI_3$) perovskite solar cells to be commercialized. Herein, we demonstrate a diffusion-engineered perovskite synthesis method using MAI/ethanol dipping, and compared it to the conventional synthesis method from MAI/iso-propanol. Diffusion of MAI/C_2H_5OH into the $PbCl_2$ film was observed to be more favorable than that of MAI/C_3H_7OH. Facile perovskite conversion from ethanol and highly-crystalline $MAPbI_3$ with minimized impurities boosted the efficiency from 5.86% to 9.51%. Additionally, we further identified the intermediates and thereby the reaction mechanisms of $PbCl_2$ converting into $MAPbI_3$. Through straightforward engineering to enhance the surface morphology as well as the crystallinity of the perovskite with even faster conversion, an initial power conversion efficiency of 11.23% was obtained, in addition to superior stability after 30 days under an ambient condition.

The feasible challenges in solar cell commercialization are enhancement in power conversion efficiency (PCE) and cost reduction to support the world-wide electricity consumption[1–5]. Alternatively, organometallic perovskite solar cells were first demonstrated by Miyasaka's group in 2009 with a PCE of 3.8%[6], and an enormous growth has been achieved over the last 6 years with the highest efficiency of 22.10%[7]. Perovskite ($CH_3NH_3PbI_3$) solar cells are settled as the most attractive topic in photovoltaic research areas due to the low fabrication cost and high efficiencies, followed by inherent advantages of the perovskite material which include an appropriate and direct bandgap, small exciton binding energy, balanced ambipolar charge transport properties, etc.[8–12]. Furthermore, the synthesis of $CH_3NH_3PbI_3$ ($MAPbI_3$) goes through a simple process, by mixing PbI_2 and MAI precursors[6]. In 2012, the superior performance via $MAPbI_3$ synthesis with $PbCl_2$ and MAI precursors was introduced by Snaith's group, and property analyses were carried out by many groups[13–16]. Since then, researchers widely studied the chlorine effect, and concluded that chlorine enhances the morphology of perovskite films[16–20]. Even though the chlorine effect is suggested by many research groups, understanding the mechanisms on the synthesis is still required to be elucidated.

Architectural challenges are widely studied due to the ambipolar behavior[21–23] of perovskites. Among them, the highest efficiency of 22.10%[7] has been achieved with mesoporous structure, and mesoporous layer allows the additional light trapping effect[24,25]. In the mesoscopic structure, there are two major $MAPbI_3$ deposition methods. The one-step solution deposition generally uses a mixture solution of PbI_2 and MAI[16], and the sequential deposition is carried out by pre-depositing the PbI_2 film, followed by dipping it into an MAI-dissolved iso-propanol solution to form the $MAPbI_3$ film[26]. Among them, the one-step solution deposition is highly beneficial in that this process is quite simple and time-saving. However, the sequential deposition is reported with a higher PCE than that of the one-step deposition[27–29] due to the enhanced pore filling through the mesoporous TiO_2 (mp-TiO_2). Although the sequential deposition guarantees a high PCE, a comparative disadvantage in the sequential deposition is that it is a long-time process, since it goes through multiple steps to fabricate the perovskite film[26].

[1]WCU Hybrid Materials Program, Department of Materials Science and Engineering, Research Institute of Advanced Materials, Seoul National University, Seoul 08826, Korea. [2]Nano Mechanical Systems Research Division, Department of Nano Mechanics, Korea Institute of Machinery & Materials (KIMM), Daejeon 305-343, Korea. Correspondence and requests for materials should be addressed to B.P. (email: byungwoo@snu.ac.kr)

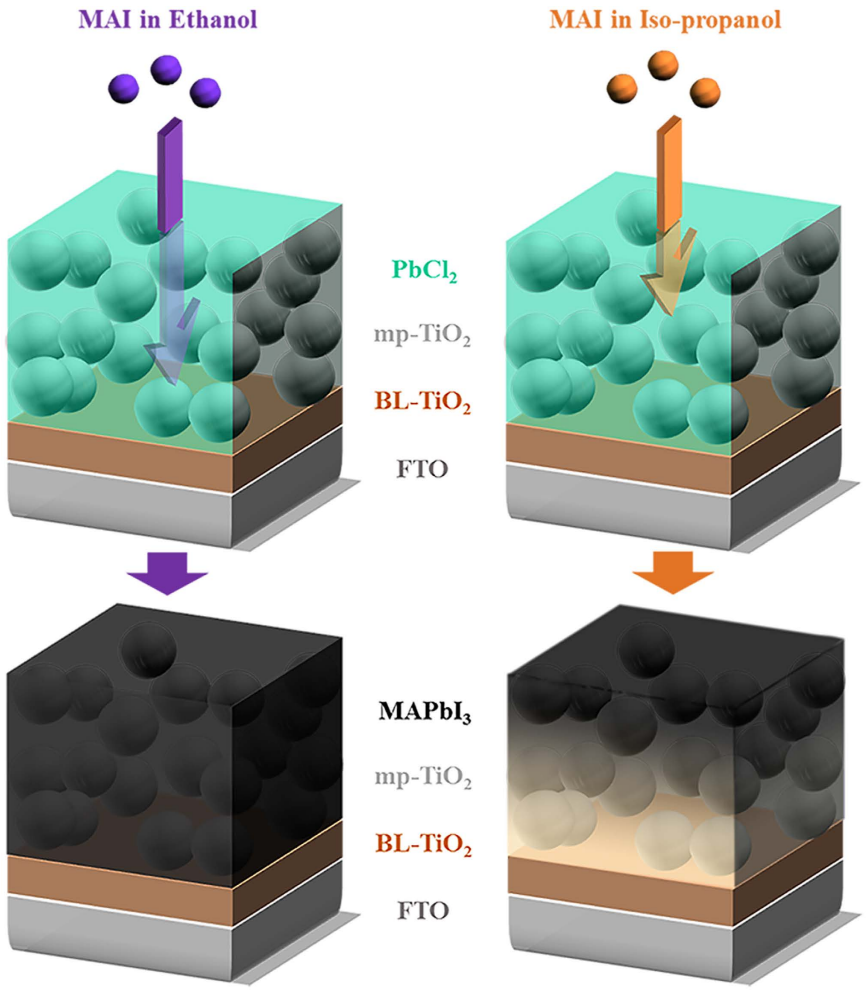

Figure 1. Schematic illustration of the MAI in ethanol or iso-propanol diffusing into the $PbCl_2$-wetted mesoporous-TiO_2 (mp-TiO_2). The blocking-layer is coated on SnO_2:F (FTO).

In this article, we have demonstrated a straightforward diffusion-controlled synthesis approach by replacing the conventional MAI-dissolved iso-propanol solution with a MAI-dissolved ethanol solution, which enhanced the crystallinity, boosted the perovskite transformation, and minimized impurities. Moreover, we have detected intermediate phases when the $PbCl_2$ precursor transforms into $MAPbI_3$, and engineered the $MAPbI_3$ deposition procedure by artificially mixing those intermediates as deposition precursors. This novel approach allowed superior surface morphology and crystallinity with enhanced conversion kinetics of $MAPbI_3$, yielding an initial PCE of 11.23% and notable stability exhibiting 10.14% PCE after 30 days under ambient conditions.

Results

Ethanol Conversion. Sequential deposition is one of the most preferable methods for perovskite fabrication due to the high PCE. One major problem, however, is the long fabrication time by multiple fabrication steps[26]. To reduce the fabrication time in the sequential deposition process, boosting the formation kinetics of $MAPbI_3$ using MAI with $PbCl_2$ precursors is required. Therefore, a low viscous solvent and larger concentration of MAI are necessary for effective diffusion of MAI into the $PbCl_2$ layer. In general, conventional dipping solution uses 10 mg mL^{-1} of MAI in iso-propanol[26], and a high concentration of MAI in solvent reduces both cuboid sizes and PCEs[30]. Thus, finding an alternative solvent is necessary for the viscosity and diffusion aspects. Figure 1 schematically illustrates the movements of ionized MAI into the $PbCl_2$ film with ethanol (20 mg mL^{-1}) and iso-propanol (10 mg mL^{-1}), where the conversion kinetics of $PbCl_2$ into $MAPbI_3$ for each solvent is quite different even with the optical images (Supplementary Fig. 1, fast conversion kinetics with MAI/ethanol). The extent of the reaction was easily estimated by color changes (E_g of $MAPbI_3 \approx 1.55$ eV). However, less viscous methanol was not effective due to the dissolution of $MAPbI_3$ (Supplementary Fig. 2)[26]. The fabricated perovskite film with the same concentration (20 mg mL^{-1}) for the iso-propanol solution results in rather small cuboid sizes (~80 nm) with a low PCE of 2.08% in the solar cell performance, as shown in Supplementary Fig. 3. The cuboid size of $MAPbI_3$ with an ethanol solution is also distinguishable from that with iso-propanol, as shown in the scanning electron microscopy (SEM) (Fig. 2a,b). The $PbCl_2$-deposited film and cuboid-size distributions are plotted in Fig. 2c, and the synthesized perovskite with twice-large cuboid sizes (~1180 nm) through an ethanol conversion is expected to produce higher carrier mobilities[31].

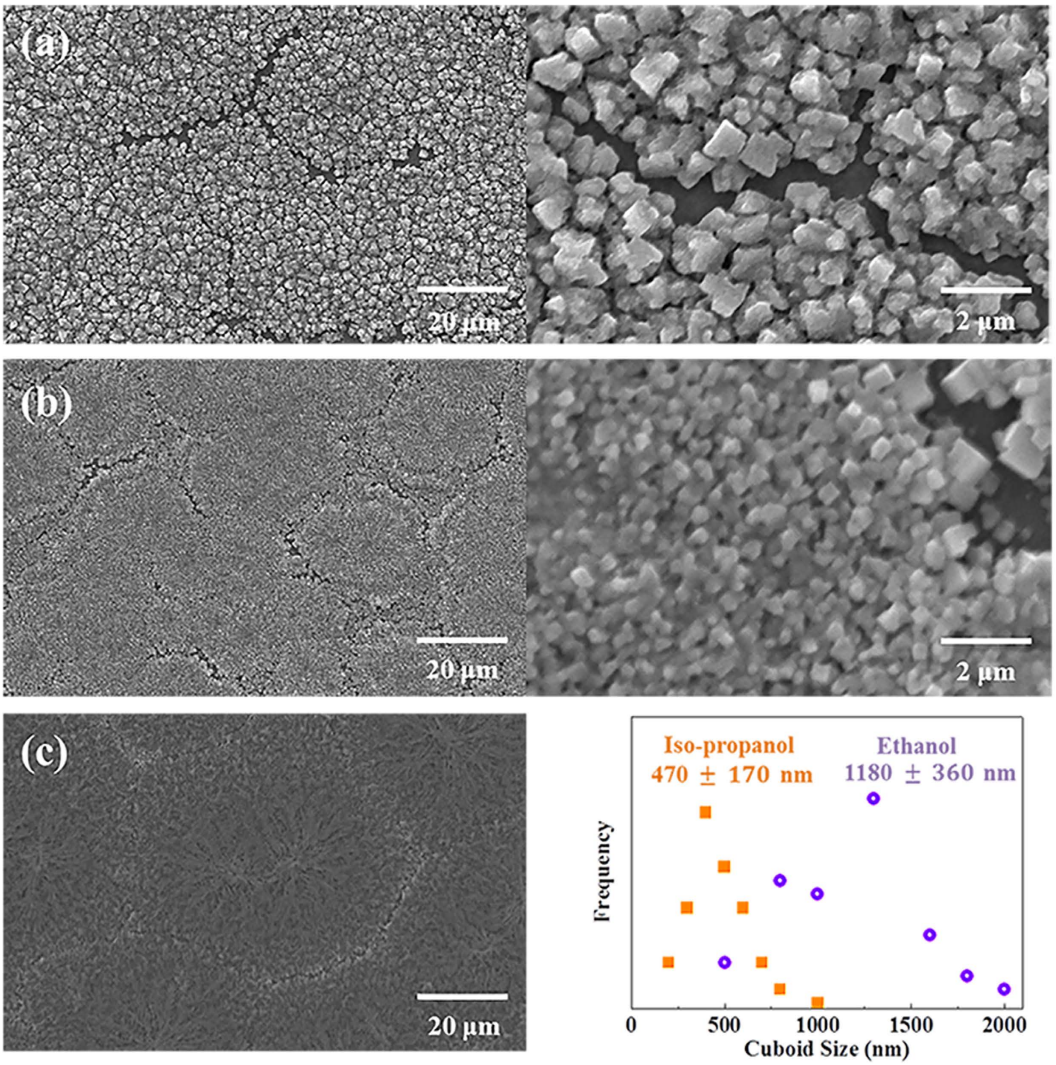

Figure 2. Solvent effects on $MAPbI_3$ using ethanol or isoporpanol. (**a**) SEM images of $MAPbI_3$ using ethanol, (**b**) $MAPbI_3$ using iso-propanol, and (**c**) $PbCl_2$ on mp-TiO_2. The average cuboid size is shown for $MAPbI_3$ by ethanol or iso-propanol.

Figure 3 illustrates qualitative analysis of the perovskite formation with ethanol or iso-propano. The energy disperse x-ray spectroscopy (EDS) was conducted to identify the chlorine concentration (Fig. 3a). $MAPbI_3$ converted from an ethanol solution contains lower Cl than that of iso-propanol-synthesized $MAPbI_3$ since unreacted $PbCl_2$ or partially-reacted $MAPbCl_3$ remains in the film. Still, ethanol-based $MAPbI_3$ shows some chlorine content, and we believe that this is caused by MACl which is a co-product during the $MAPbI_3$ synthesis[16–18]. Actually, there is a possibility that chlorine is doped in the perovskite structure ($MAPbI_{3-x}Cl_x$) as reported by several groups[14–16]. However, the small quantity of chlorine in the perovskite structure is difficult to be evaluated, and the remaining chlorine may form other products[17,19]. Cross-sectional SEM image of $MAPbI_3$ perovskite solar cell by ethanol exhibits uniform film structures, as shown in Fig. 3b. For further understanding of impurities, X-ray diffraction (XRD) scans were compared, and an ethanol-based $MAPbI_3$ shows clear (110), (220) and (330) peaks (Fig. 3c). On the contrary, the conversion with iso-propanol produced impurity peaks of PbI_2 and $MAPbCl_3$ (Fig. 3c), indicating incomplete reaction. To explain the effect of ethanol on the crystallinity, we have additionally confirmed that the longer dipping time increases the crystallinity of $MAPbI_3$ (Supplementary Fig. 4) eVen when the reaction was completed. Together with the optical observation in Supplementary Fig. 1, it can be said that MAI/ethanol-converted $MAPbI_3$ completes the reaction faster with better crystallinity, compared to that of iso-propanol for the same dipping time. Furthermore, the light absorption from the synthesized perovskite is clearly different between ethanol and iso-propanol (Fig. 3d). The enhanced absorption at approximately 800 nm by ethanol is due to the superior purity of $MAPbI_3$ ($E_g \approx 1.55$ eV), while partially-reacted MAPbI3 by iso-propanol contains high-bandgap impurities, such as PbI2 ($E_g \approx 2.36$ eV)[32] and $MAPbCl_3$ ($E_g \approx 3.17$ eV)[33]. Therefore, the overall PCE is greatly improved from 5.86% to 9.51% (Fig. 3e) with much better stability (Fig. 3f), and both methods performed high reproducibility (Supplementary Fig. 5 and Supplementary Table 1). After 30 days, the PCE decreased from 9.51% to 8.53% and 5.86% to 3.75%, respectively, for the ethanol and iso-propanol

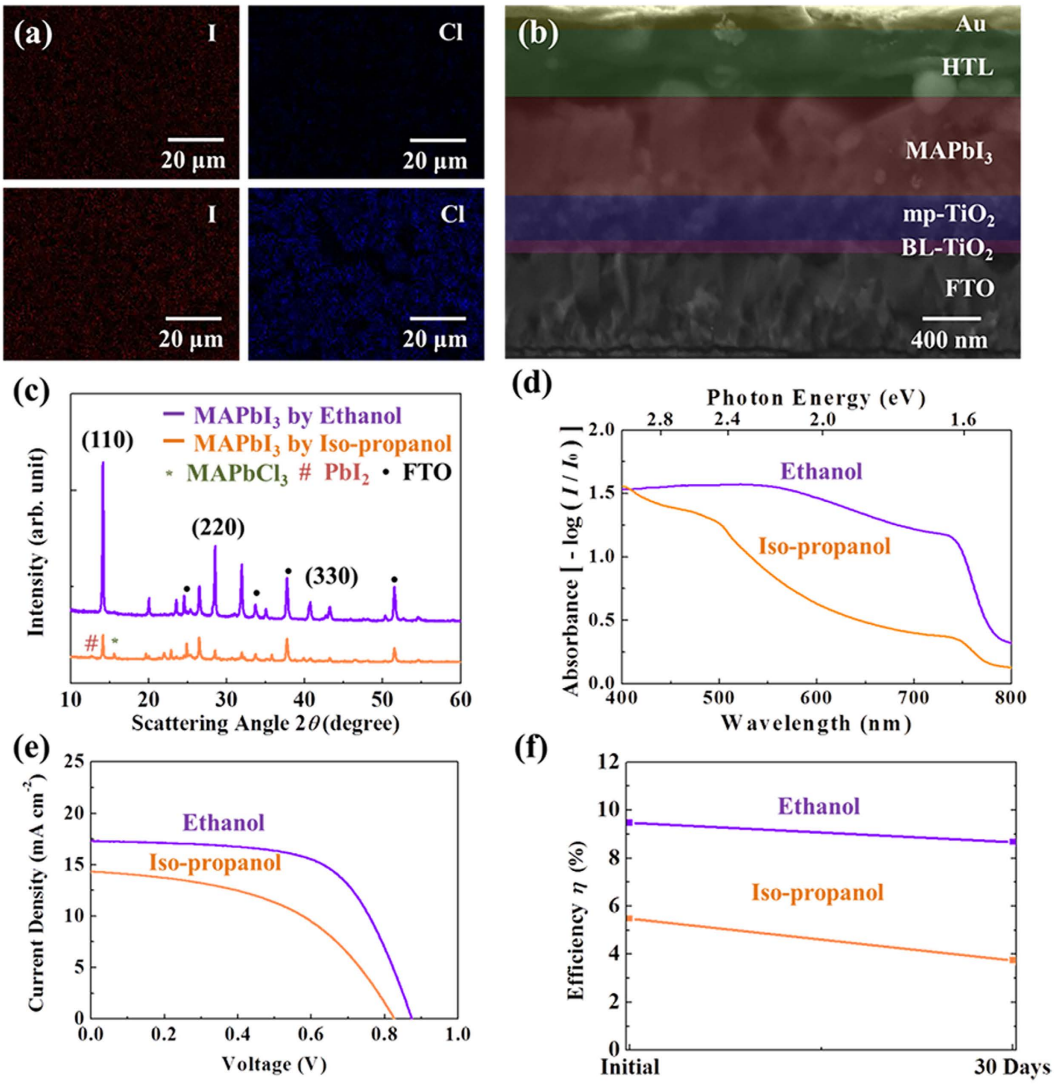

Figure 3. The dependence of $MAPbI_3$ perovsktie solar cells using the MAI in an ethanol or iso-propanol solution. (**a**) EDS mapping for iodine and chlorine in the synthesized $MAPbI_3$ with an ethanol (top) or iso-propanol (bottom) solution. (**b**) Cross-sectional SEM image of a $MAPbI_3$ perovskite solar cell from the MAI/ethanol solution. (**c**) X-ray diffraction of $MAPbI_3$. (**d**) Absorption spectra for the synthesized $MAPbI_3$. (**e**) *J-V* characteristics of the $MAPbI_3$ perovskite solar cells. (**f**) Degradation of solar cells synthesized by ethanol or iso-propanol for the as-fabricated cells and cells after 30 days.

Reaction Condition		V_{oc} (V)	J_{sc} (mA/cm^2)	*FF*	η (%)
Initial	Ethanol	0.87	17.3	0.63	9.51
	Iso-propanol	0.83	14.4	0.49	5.86
30 Days	Ethanol	0.84	16.4	0.63	8.53
	Iso-propanol	0.79	10.1	0.47	3.75

Table 1. Photovoltaic performance of $MAPbI_3$ perovskite solar cells using an ethanol or iso-propanol solution (as-fabricated cells and cells after 30 days).

solution (Table 1). The improved crystallinity and enlarged grain of $MAPbI_3$ by ethanol surely prevents possible air penetration through various grain boundaries, leading to stability enhancement. The half-lifetime of the $MAPbI_3$ perovskite solar cell (degradation details in Supplementary Fig. 6) was estimated to be ~150 and ~40 days, respectively, for ethanol and iso-propanol.

To identify the reaction mechanisms, intermediate phases during the perovskite formation were investigated by the concentration variations of MAI in ethanol. With a low concentration of MAI/ethanol (Fig. 4a), $PbCl_2$ partially reacts into PbI_2 (5 mg mL^{-1}). The chlorine in $PbCl_2$ ion-exchanges with iodine in MAI to form PbI_2, and the

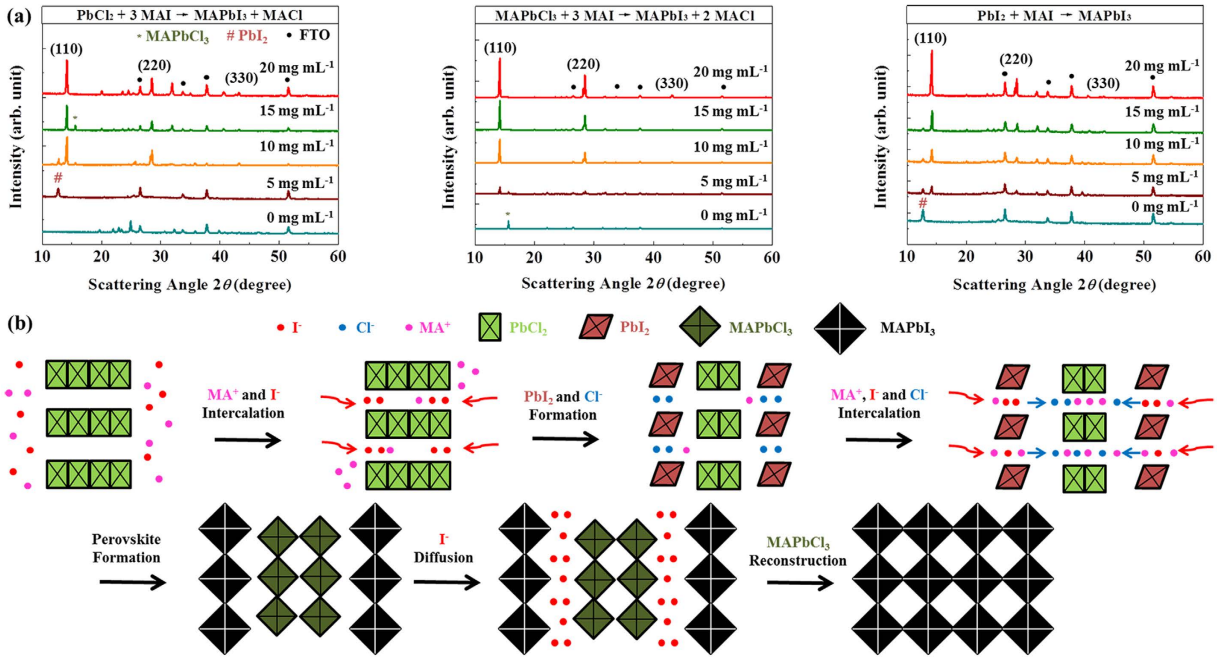

Figure 4. Reaction intermediates and mechanism analysis by X-ray diffraction measurements. (**a**) Reaction 1 (left), reaction 4 (middle), and PbI_2 precursor (right) with various concentrations of MAI in an ethanol solution. (**b**) Mechanisms of reaction 1 ($PbCl_2 + 3\,MAI \rightarrow MAPbI_3 + 2\,MACl$). The MAI and ethanol diffuse into the outer $PbCl_2$ layer, which converts $PbCl_2$ into PbI_2 and MACl. Additional MAI from the solution converts the synthesized outer PbI_2 into $MAPbI_3$, and MACl reacts with the inner $PbCl_2$ transforming into $MAPbCl_3$. The synthesized $MAPbCl_3$ ion-exchanges with I^- for the full $MAPbI_3$ and MACl to complete the reaction.

dissociated MA^+ and Cl^- from outer $PbCl_2$ intercalate into the inner $PbCl_2$ layer, transforming to the $MAPbCl_3$ phase (15 mg mL^{-1} of MAI/ethanol). The intermediate PbI_2 reacts with MAI directly to form $MAPbI_3$ by intercalating MAI in the layered PbI_2, while $MAPbCl_3$ will ion-exchange with I^- and reconstructs to the final $MAPbI_3$, as schemed in Fig. 4b (20 mg mL^{-1} of MAI/ethanol). The whole reaction occurs through the following steps:

$$2\ PbCl_2 + 2\ MAI \rightarrow PbI_2 + PbCl_2 + 2\ MACl\ (step\ 1)$$

$$PbI_2 + MAI \rightarrow MAPbI_3\ (step\ 2)$$

$$PbCl_2 + 2\ MACl \rightarrow MAPbCl_3 + MACl\ (step\ 3)$$

$$MAPbCl_3 + MACl + 3\ MAI \rightarrow MAPbI_3 + 4\ MACl\ (step\ 4)$$

$$PbCl_2 + 3\ MAI \rightarrow MAPbI_3 + 2\ MACl.\ (Total\ Reaction)$$

The PbI_2 phase converts into $MAPbI_3$ earlier than the formation of $MAPbCl_3$, as shown by the X-ray diffraction of $MAPbI_3$ vs. $MAPbCl_3$ phases for MAI concentrations of 10 and 15 mg mL^{-1} (Fig. 4a). We have also compared the perovskite formation from $MAPbCl_3$ ($MAPbCl_3 + 3\,MAI \rightarrow MAPbI_3 + 3\,MACl$) with PbI_2 ($PbI_2 + MAI \rightarrow MAPbI_3$) (respectively, in the middle and right of Fig. 4a), and found that both have resulted in no intermediate phases. Synthesizing fully-converted $MAPbI_3$ from $PbCl_2$ requires both intercalation and reconstruction steps, while the idea of reconstruction from $MAPbCl_3$ to $MAPbI_3$ was investigated in the previous report[34]. Therefore, we intuitively conclude that the recrystallization of intermediates both inside and on top of the mp-TiO_2 film can enhance the coverage morphology, nanostructures, and crystallinity[16–18] of $MAPbI_3$ by multiple crystal-alignment steps. Moreover, ethanol conversion increases the kinetics of the reaction steps, and produces improved $MAPbI_3$ film, compared to the conversion with iso-propanol.

Reaction Mechanism Engineering. To understand the phase-formation paths of $MAPbI_3$ from $PbCl_2$, we came up with an idea to further optimize $MAPbI_3$ by utilizing the identified intermediate phases. While the direct conversion of $MAPbCl_3$ to $MAPbI_3$ can drastically reduce the reaction time, the repetition of crystallization from $PbCl_2$ to $MAPbI_3$ will enhance the surface morphology. Even though PbI_2 appears during the transformation of the $PbCl_2$ precursor to $MAPbI_3$, and increases the reaction kinetics, the $MAPbCl_3$ precursor is more reactive than the PbI_2 precursor to synthesize $MAPbI_3$ (middle and right graphs in Fig. 4a) where the $MAPbCl_3$ precursor is likely to transform with lower MAI concentration than that of the PbI_2 precursor. Also, the chlorine-based

	Reaction Mechanism	Precursor Ratio ($PbCl_2$: $MAPbCl_3$)
RXN 1	$PbCl_2 + 3\ MAI \rightarrow MAPbI_3 + 2\ MACl$	3:0
RXN 2	$2\ PbCl_2 + MAPbCl_3 + 9\ MAI \rightarrow 3\ MAPbI_3 + 7\ MACl$	2:1
RXN 3	$PbCl_2 + 2\ MAPbCl_3 + 9\ MAI \rightarrow 3\ MAPbI_3 + 8\ MACl$	1:2
RXN 4	$MAPbCl_3 + 3\ MAI \rightarrow MAPbI_3 + 3\ MACl$	0:3

Table 2. Precursor ratio of $PbCl_2$: $MAPbCl_3$ for the reactions 1, 2, 3, and 4.

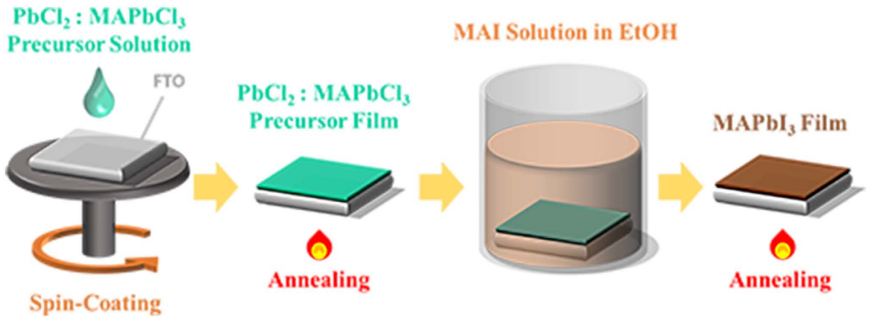

Figure 5. Schematic illustration of the experimental procedure. Various ratios of $PbCl_2$: $MAPbCl_3$ were initially deposited on the substrate, and then the MAI-dissolved ethanol solution was utilized to synthesize $MAPbI_3$.

precursor should be preferred considering the positive effects of chlorine on the $MAPbI_3$ perovskite solar cells[16–20]. Therefore, a straightforward direction is rendered by mixing $PbCl_2$ and $MAPbCl_3$ in several different ratios of 3:0 (reaction 1), 2:1 (reaction 2), 1:2 (reaction 3), and 0:3 (reaction 4), to optimize the reaction time with smooth surface morphology (Table 2 and Fig. 5).

As expected, we observed the morphology changes by synthesizing $MAPbI_3$ films from precursors with different ratios of $PbCl_2$ and $MAPbCl_3$ through SEM, as shown in Fig. 6a. Perovskite films synthesized by reaction 2 exhibits clearly improved coverage with ~2320-nm-sized cuboids. Furthermore, addition of $MAPbCl_3$ (reaction 3 and 4) deteriorates the coverage, but increases the cuboid size. When a larger amount of the $MAPbCl_3$ precursor is added through reactions, the crystallinity of $MAPbI_3$ is enhanced significantly, as shown by XRD (Fig. 6b,c). The enhanced crystallinity can be explained by the extent of reaction, and the facilely-transformed perovskite is likely to have high crystallinity even with the same dipping time (Supplementary Fig. 4). These observations are also consistent with the optical variations during the $MAPbI_3$ formation (Supplementary Fig. 7). It should be noted that the coverages for the reactions 1, 2, 3, and 4 are different. However, conversions at ~10 s are distinct between reactions 1 ($PbCl_2$ precursor) and 4 ($MAPbCl_3$ precursor). The light absorption in Fig. 6d indicates that the absorption is more influenced by the coverage rather than the crystallinity and cuboid size of $MAPbI_3$. The maximum coverage in reaction 2 reached the highest absorption, and the minimum coverage with reaction 4 yielded the lowest absorption. As a material perspective, $MAPbI_3$ synthesis by reaction 4 is supposed to show excellent properties due to the high crystallinity and cuboid sizes, as plotted in Fig. 7a. Moreover, EDS was additionally measured to identify the comparative chlorine contents with iodine, which is plotted in Fig. 7b for each reaction, indicating that reaction 1 obtained the highest, and reaction 4 occupied the lowest concentration of chlorine. This chlorine tendency suggests that a co-product of MACl is minimized through the addition of $MAPbCl_3$. (It should be noted that the EDS technique may not reflect the accurate chlorine concentration due to the coverage difference of each reaction.) It is possible that the detected chlorine through EDS is from the MACl phase or other products[16–18]. Moreover, excessive chlorine may lead to impurities, and deteriorate the device performance. Therefore, high crystallinity and low impurity of $MAPbI_3$ are highly beneficial in the carrier mobilities, but recombination of carriers arising from poor coverage[31] is another factor that we should be aware of.

To understand the effects of crystallinity and coverage on the photovoltaic performance and stability, *J-V* curves are measured for 30 days under ambient conditions (Supplementary Fig. 6, and Table 3). In Fig. 7c, *J-V* curves were shown for the performance of the solar cells from each reaction, and the highly covered perovskite film from reaction 2 achieved the highest PCE of 11.23%. The lowest PCE of 4.03% was obtained by reaction 4, and these results indicate that the initial PCE is highly dependent on the perovskite coverage, which plays crucial roles in the carrier recombination. In contrast, $MAPbI_3$ synthesized by reaction 4 was distinctively stable after 30 days. The stability is well correlated with the crystallinity and grain size, apparent from the normalized PCE in Fig. 7d, confirming the reduced decomposition behavior from the low-defect perovskite. All of the solar cells with different experimental conditions performed high reproducibility (Supplementary Fig. 5 and Supplementary Table 1). From the reactions 1, 2, 3, and 4, the half-lifetimes of $MAPbI_3$ perovskite solar cells (degradation details in Supplementary Fig. 6) are estimated to be ~150, ~160, ~270, and ~300 days.

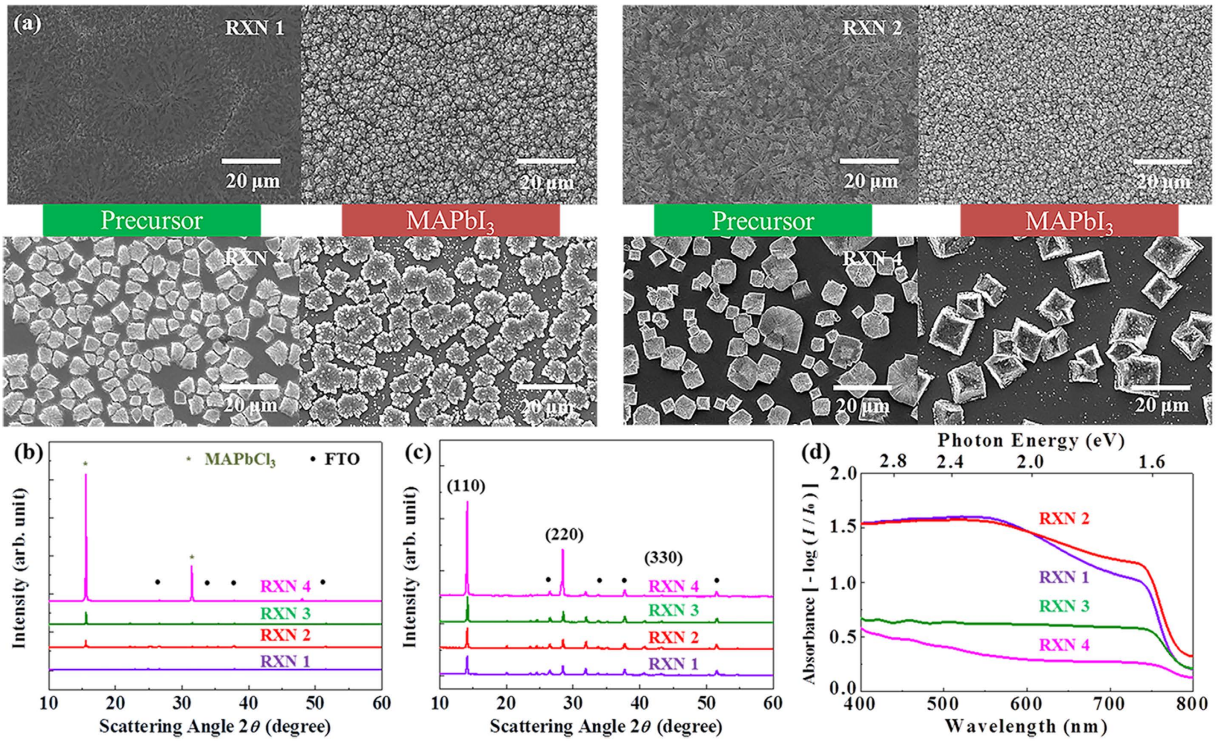

Figure 6. The film quality dependence of $MAPbI_3$ for the reactions 1, 2, 3, and 4. (**a**) SEM images of the precursor and $MAPbI_3$, (**b,c**) X-ray diffraction for the precursor and $MAPbI_3$, and (**d**) absorption spectra of $MAPbI_3$ by reactions 1, 2, 3, and 4.

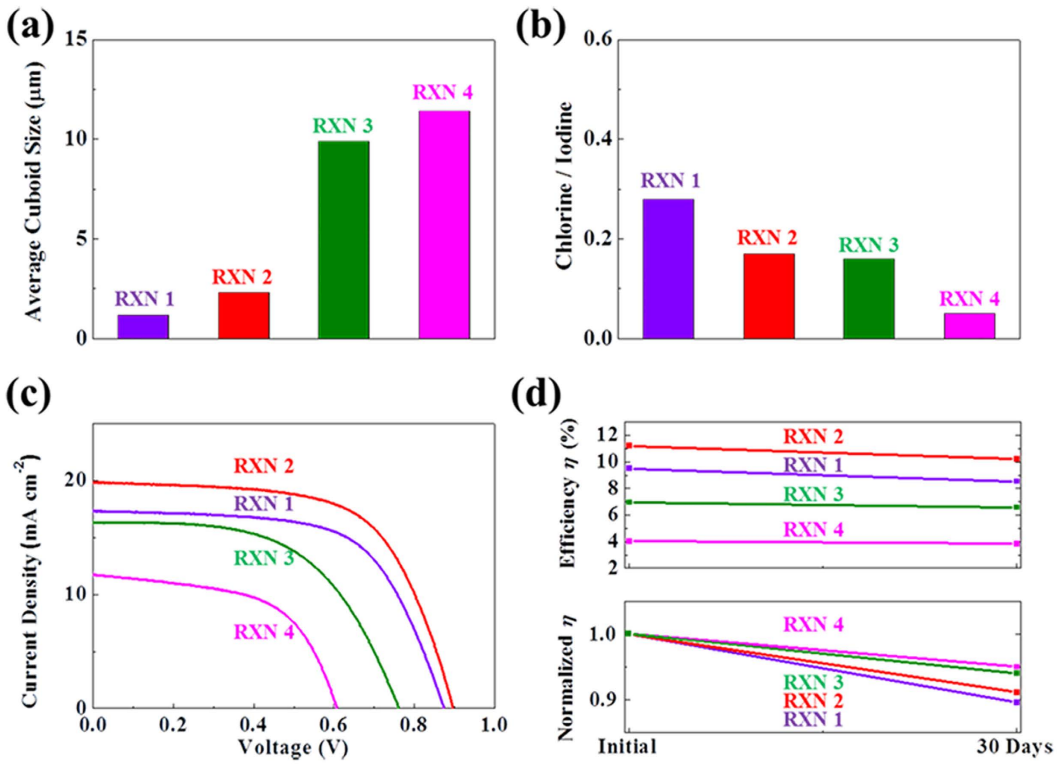

Figure 7. The purity and deivce performance analysis for the reactions 1, 2, 3, and 4. (**a**) Average cuboid size, (**b**) EDS for the comparative chlorine contents with iodine contents, (**c**) *J-V* curves, and (**d**) the efficiency degradation for the as-fabricated cells and cells after 30 days.

Reaction Conditions		V_{oc} (V)	J_{sc} (mA cm^{-2})	*FF*	η(%)
Initial	RXN 1	0.87	17.3	0.63	9.51
	RXN 2	0.90	19.8	0.63	11.23
	RXN 3	0.76	16.3	0.56	6.94
	RXN 4	0.61	11.7	0.57	4.03
30 Days	RXN 1	0.84	16.4	0.62	8.53
	RXN 2	0.89	17.8	0.64	10.14
	RXN 3	0.73	15.2	0.59	6.55
	RXN 4	0.61	11.7	0.52	3.83

Table 3. Solar cell performance from the reactions 1, 2, 3, and 4 (as-fabricated cells and cells after 30 days).

Discussion

Fast conversion can have positive influences on the device performance and stability by producing highly-crystalline $MAPbI_3$ perovskite. Therefore, we have controlled the diffusion reaction of MAI and $PbCl_2$ with ethanol to boost the perovskite transformations, leading to phase-pure and highly-crystalline perovskite films. Since $PbCl_2$ goes through several intermediate phases during the formation of $MAPbI_3$, we utilized the intermediates by mixing them with a conventional $PbCl_2$ precursor to boost the conversion kinetics and performance of the resulting solar cell. Thereby, the optimized crystallinity and coverage yielded a PCE of 11.23% with $PbCl_2$: $MAPbCl_3 = 2{:}1$ (reaction 2). Although the precursor with 100% $MAPbCl_3$ (reaction 4) resulted in the fastest transformations of $MAPbI_3$ and the most stable solar cell performance, poor coverage lowered the PCE of the device. Therefore, compact coverage of the perovskite with super-sized cuboids expects to achieve further enhanced performance and stability of the $MAPbI_3$ perovskite solar cell. At this point, investigation of hysteresis still remains as a future work.

Methods

Perovskite Solar Cell Fabrication. Fluorine-doped tin oxide substrate (FTO, TEC 8: Pilkington) was cleaned by sonication in Mucasol (Aldrich), ethanol (DEAJUNG), and DI water for 30 min sequentially. 50 nm of compact the TiO_2 blocking layer was deposited by spin-coating the mixture solution of 0.15 mM titanium diisopropoxide bis(acetylacetonate) (Aldrich) and 1-butanol (75.0 wt. % in iso-propanol, Aldrich) in 2500 rpm for 20 s followed by heating at 125 °C for 5 min in an air oven. The same step was repeated with 0.3 mM concentration and the substrate was annealed at 500 °C for 30 min. After the TiO_2 blocking layer was ready, TiO_2 pastes (ENB Korea) with 20 nm-sized nanoparticles were mixed with terpineol (Aldrich) in 1:2 ratio, followed by spin-coating at 4000 rpm for 30 s, yielding a ~350 nm thickness of the mp-TiO_2 layer. For the perovskite synthesis, MAI was first synthesized by following literature method[26]. 1.5 M $PbCl_2$ (Aldrich) was diluted in dimethyl sulfoxide (DMSO, Aldrich), and then MACl (Aldrich) was added with different concentrations (0, 0.5, 1.0, and 1.5 M) to synthesize the reaction 1, 2, 3, and 4 precursors where the reaction 1, 2, and 3 precursors contain both $MAPbCl_3$ and $PbCl_2$ phases, whereas the reaction 4 precursor contains only $MAPbCl_3$ ($MAPbCl_3$ forms by 1:1 molar stoichiometric ratios of MACl and $PbCl_2$). After the preparation of precursor mixture solutions, the solution was preheated at 100 °C and the substrate was preheated at 150 °C, then the solution was spin-coated at 2000 rpm for 5 s, followed by 6000 rpm for 5 s. The film was annealed at 150 °C for 30 min, and cooled down in an ambient condition. After the film was cooled down, it was dipped into 20 mg mL^{-1} of MAI in an anhydrous ethanol solution (Daejung) for 20 min under ambient conditions (25 °C and 55% humidity) and annealed at 100 °C for 30 min. The hole transport solution was prepared by mixing 72.3 mg mL^{-1} of spiro-OMeTAD (Merck) in chlorobenzene (Aldrich) with 28.8 μL of *tert*-butylpyridine (Aldrich) and a 17.5 μL solution of 520 mg of lithium *bis*(trifluoromethylsyfonyl) imide salt (Aldrich) in 1 mL acetonitrile (Aldrich) was spin-coated at 3000 rpm for 45 s. Finally, 100 nm thickness of an Au electrode was then thermally evaporated.

Device Characterizations. The morphologies of $MAPbI_3$ perovskite films were analyzed using scanning electron microscope (Normal-SEM, JSM-6360: Hitachi). The chlorine compositions and distribution were examined using energy-dispersive X-ray spectroscopy (EDS, ISIS-300: Oxford Instruments). The phases of the synthesized samples were characterized by X-ray diffraction (XRD, D8 Advance: Bruker). The photocurrent-voltage (*J*–*V*) curves of $MAPbI_3$ perovskite solar cells were obtained with a potentiostat (CHI 608C: CH Instrumental Inc.) under AM 1.5 illumination at 100 mW cm^{-2} (K3000: McScience) with an active cell area of 0.09 cm^2. The field-emission scanning electron microscope (FE-SEM, Merlin-Compact: Carl Zeiss) was used to observe the plan and cross-sectional views. The absorption spectra of the $MAPbI_3$-deposited films were recorded on a UV-Vis spectrophotometer (Lambda 20: Perkin Elmer). Stability was measured every 5 days, and stored at 25 °C with 55% of humidity under dark conditions.

References

1. Shin, B. *et al.* Thin film solar cell with 8.4% power conversion efficiency using an earth-abundant Cu_2ZnSnS_4 absorber. *Prog. Photovolt.: Res. Appl.* **21,** 72–76 (2013).
2. Choi, H. *et al.* The role of ZnO-coating-layer thickness on the recombination in CdS quantum-dot-sensitized solar cells. *Nano Energy* **2,** 1218–1224 (2013).
3. Kim, D. *et al.* Backcontact CdSe/CdTE windowless solar cells. *Sol. Energ. Mat. Sol. C.* **109,** 246–253 (2013).

4. Kim, J. *et al.* The role of a $TiCl_4$ treatment on the performance of CdS quantum-dot-sensitized solar cells. *J. Power Sources* **220,** 108–113 (2012).
5. Choi, H. *et al.* The construction of tandem dye-sensitized solar cells from chemically-derived nanoporous photoelectrodes. *J. Power Sources* **274,** 937–942 (2015).
6. Kojima, A., Teshima, K., Shirai, Y. & Miyasaka, T. Organometal halide perovskites as visible-light sensitizers for photovoltaic cells. *J. Am. Chem. Soc.* **131,** 6050–6051 (2009).
7. National Renewable Energy Laboratory (NREL), Best Research-Cell Efficiencies, http://www.nrel.gov/ncpv/images/efficiency_chart.jpg (Accessed: 30th March, 2016).
8. Kazim, S., Nazerruddin M. K., Gratzel, M. & Ahmad, S. Perovskite as Light Harvester: A Game Charger in Photovoltaics. *Angew. Chem. Int. Ed.* **53,** 2812–2824 (2014).
9. McGehee, M. D. Materials science: fast-track solar cells. *Nature* **501,** 323–325 (2013).
10. Hodes, G. Perovskite-based solar cells. *Science* **342,** 317–318 (2013).
11. Ponseca, C. S. *et al.* Organometal halide perovskite solar cell materials rationalized: ultrafast charge generation, high and microsecond-long balanced mobilities, and slow recombination. *J. Am. Chem. Soc.* **136,** 5189–5192 (2014).
12. Frost, J. M. *et al.* Atomistic origins of high-performance in hybrid halide perovskite solar cells. *Nano Lett.* **14,** 2584–2590 (2014).
13. Lee, M. M., Teuscher, J., Miyasaka, T., Murakami, T. N. & Snaith, H. J. Efficient hybrid solar cells based on meso-superstructured organometal halide perovskites. *Science* **338,** 643–647 (2012).
14. Colella, S. *et al.* $MAPbI_{3-x}Cl_x$ mixed halide perovskite for hybrid solar cells: the role of chloride as dopant on the transport and structural properties. *Chem. Mater.* **25,** 4613–4618 (2013).
15. Wehrenfennig, C., Eperon, G. E., Johnston, M. B., Snaith, H. J. & Herz, L. M. High charge carrier mobilities and lifetimes in organolead trihalide perovskites. *Adv. Mater.* **26,** 1584–1589 (2014).
16. Williams, S. T. *et al.* Role of chloride in the morphological evolution of organo-lead halide perovskite thin films. *ACS Nano* **8,** 10640–10654 (2014).
17. Unger, E. L. *et al.* Chloride in lead chloride-derived organo-metal halides for perovskite-absorber solar cells. *Chem. Mater.* **26,** 7158–7165 (2014).
18. Deepa, M., Ramos, J. F., Shivaprasad M. S. & Ahmad, S. Unravelling the Role of Monovalent Halides in Mixed-Halide Organic-Inorganic Perovskite. *ChemPhysChem.* **17,** 913–920 (2016).
19. Yin, W.-J., Chen H., Shi, T., Wei, S.-H. & Yan, Y. Origin of high electronic quality in structurally disordered $CH_3NH_3PbI_3$ and the passivation effect of Cl and O at grain boundaries. *Adv. Electron. Mater.* **1,** 1500044 (2015).
20. Mosconi, E., Ronca, E. & Angelis, F. D. First-principles investigation of the TiO_2/organohalide perovskites interface: the role of interfacial chlorine. *J. Phys. Chem. Lett.* **5,** 2619–2625 (2014).
21. Chen, Q. *et al.* Planar heterojunction perovskite solar cells via vapor-assisted solution process. *J. Am. Chem. Soc.* **136,** 622–625 (2013).
22. Eperon, G. E., Burlakov, V. M., Docampo, P., Goriely, A. & Snaith, H. J. Morphological control for high performance, solution-processed planar heterojunction perovskite solar cells. *Adv. Funct. Mater.* **24,** 151–157 (2014).
23. Liu, M., Johnston, M. B. & Snaith, H. J. Efficient planar heterojunction perovskite solar cells by vapour deposition. *Nature* **501,** 395–398 (2013).
24. Mihi, A. Zhang, C. & Braun, P. V. Transfer of preformed three-dimensional photonic crystals onto dye-sensitized solar cells. *Angew. Chem. Int. Ed.* **50,** 5712–5715 (2011).
25. Grandidier J., Callahan, D. M., Munday, J. N. & Atwater, H. A. Light absorption enhancement in thin-film solar cells using whispering gallery modes in dielectric nanospheres. *Adv. Mater.* **23,** 1272–1276 (2011).
26. Burschka, J. *et al.* Sequential deposition route to high performance perovskite-sensitized solar cells. *Nature* **499,** 316–320 (2013).
27. Im, J.-H., Kim, H.-S. & Park, N.-G. Morphology-photovoltaic property correlation in perovskite solar cells: one-step versus two-step deposition of $CH_3NH_3PbI_3$. *APL Mater.* **2,** 081510 (2014).
28. Ma, Y. *et al.* A highly efficient mesoscopic solar cell based on $CH_3NH_3PbI_{3-x}Cl_x$ fabricated via sequential solution deposition. *Chem. Commun.* **50,** 12458–12461 (2014).
29. Yantara, N. *et al.* Loading of mesoporous titania films by $CH_3NH_3PbI_3$ perovskite, single step vs. sequential deposition. *Chem. Commun.* **51,** 4603–4606 (2015).
30. Im, J.-H., Jang, I.-H., Pellet, N., Gratzel, M. & Park, N.-G. Growth of $CH3NH_3PbI_3$ cuboids with controlled size for high-efficiency perovskite solar cells. *Nat. Nanotechnol.* **9,** 927–932 (2014).
31. Nie, W. *et al.* High-efficiency solution-processed perovskite solar cells with millimeter-scale grains. *Science* **347,** 522–525 (2015).
32. Supasai, T., Rujisamphan, N., Ullrich, K., Chemseddine, A. & Dittrich, T. Formation of a passivating $CH_3NH_3PbI_3/PbI_2$ interface during moderate heating of $CH_3NH_3PbI_3$ layers. *Appl. Phys. Lett.* **103,** 183906–1 (2013).
33. Comin, R. *et al.* Structural, optical, and electronic studies of wide-bandgap lead halide perovskites. *J. Mater. Chem. C* **3,** 8839–8843 (2015).
34. Zhou, H. *et al.* Interface engineering of highly efficient perovskite solar cells. *Science* **345,** 542–546 (2014).

Acknowledgements

This work was supported by the National Research Foundation of Korea (NRF): 2013R1A1A2065793, 2010-0029065 and 2015K2A1A2070386.

Author Contributions

J.K. fabricated the solar cell devices, designed the whole experiments, and participated in writing the paper. T.H. supported the optimization process on the solar cell fabrication, and participated in writing the paper. S.L. carried out the electrochemical analyses, and participated in writing the paper. B.L. supported the optimization process of $MAPbI_3$ perovskite synthesis, and participated in writing the paper with vital comments. J.K. analyzed electrochemical properties of the $MAPbI_3$ perovskite, and participated in writing the paper. G.S.J. supported the optimization steps in thermal evaporation of an Au electrode. S.N. helped writing the paper, and gave constructive scientific comments. B.P. advised on the overall experiments with vital comments, and finalized the manuscript.

Additional Information

Supplementary information accompanies this paper at http://www.nature.com/srep

Competing financial interests: The authors declare no competing financial interests.

How to cite this article: Kim, J. *et al.* Solvent and Intermediate Phase as Boosters for the Perovskite Transformation and Solar Cell Performance. *Sci. Rep.* **6**, 25648; doi: 10.1038/srep25648 (2016).